198671: garnet-bearing cordierite pelitic gneiss, Mount Narryer

(Narryer Terrane, Yilgarn Craton)

Korhonen, FJ, Fielding, IOH and Kelsey, DE

Location and sampling

Byro (SG 50-10), Chulyawarra (2144)

MGA Zone 50, 440332E 7068444N

WAROX site FJKBGD198671

Sampled on 16 June 2010

This sample was collected from a boulder in a stream bed on the east flank of the Mount Narryer Range on Boolardy Station, about 7.9 km northeast of Lanes Well, 5.5 km north of Elizabeth Springs Well, and 3.0 km northeast of Mount Narryer. The sample was collected as part of the Geological Survey of Western Australia's (GSWA) 2003–14 Yilgarn Craton Metamorphic Project, and referred to in that study as sample BG10-70c. The results from this project have not been released by GSWA, although select data have been published in Goscombe et al. (2019).

Geological context

The unit sampled is a pelitic gneiss of the Narryer Terrane in the northwest Yilgarn Craton (Myers, 1990; Wilde and Spaggiari, 2007). The Narryer Terrane includes rocks with U–Pb zircon ages ranging up to c. 3750 Ma (Kinny et al., 1988; Kemp et al., 2019), the oldest known rocks in Australia, and detrital zircons up to c. 4404 Ma, the oldest terrestrial material on Earth (Wilde et al., 2001). The Narryer Terrane consists of granite and granitic gneiss interleaved with sedimentary, mafic–ultramafic intrusive rocks, and banded iron-formation, metamorphosed at greenschist to granulite facies (Myers and Williams, 1985). A pelitic gneiss from this locality yielded a conservative maximum depositional age of 3343 ± 17 Ma and an age of metamorphism of 2659 ± 3 Ma (GSWA 198669, Lu et al., 2015a), and a quartzite, sampled about 2 km to the west-northwest, yielded a maximum depositional age of 3340 ± 20 Ma (GSWA 198654, Lu et al., 2015b). Monazite from the sample reported here yielded a weighted mean $^{207}Pb/^{206}Pb$ date of 2658 ± 9 Ma, interpreted as the age of high-grade metamorphism (GSWA 198671, preliminary data).

Petrographic description

The sample is a foliated, medium- to coarse-grained pelitic gneiss (Fig. 1) containing about 30% quartz, 27% biotite, 24% cordierite, 10% plagioclase, 5% muscovite, 2% garnet, 2% chlorite, trace aluminosilicate and K-feldspar, and accessory zircon, monazite, and apatite (Fig. 2; Table 1). The matrix has a polygonal granoblastic texture composed of aligned biotite, quartz, cordierite, and altered plagioclase. Quartz forms elongate and slightly strained grains up to 3 mm in size. Rare thin films of quartz occur around embayed biotite (Fig. 3a). Orange-red to straw brown biotite occurs as elongate laths up to 3 mm in length that define the foliation (Fig. 3b), and as smaller elongate inclusions in cordierite and garnet. Some biotite grains in the matrix are partially replaced by chlorite along cleavage planes. Cordierite forms elongate grains up to 9 mm in length that commonly host inclusions of fine-grained aligned sillimanite, and rounded quartz and biotite (Fig. 3b). Cordierite and garnet porphyroblasts are typically in textural equilibrium (Fig. 3b), although cordierite also occurs as thin symplectic intergrowths with biotite and as moats that enclose embayed biotite and garnet (Fig. 3c). Plagioclase occurs as elongate lenses of strained polygonal granoblastic aggregates partially replaced by muscovite and sericite (Fig. 3d). Muscovite is fine-grained and is restricted to these plagioclase-rich aggregates. Garnet occurs as irregular-shaped porphyroblasts up to 3.5 mm in size with rare inclusions of rounded to elongate quartz and biotite and rare trails of sillimanite (Fig. 2).

Rare small grains of rounded garnet are included within cordierite (Fig. 3c). Sparse chlorite occurs in fractures within garnet and along cleavage planes in biotite. Sillimanite is only present as aligned inclusions in garnet and cordierite; this observation was also described by Goscombe et al. (2015) for a different thin section from this sample. K-feldspar is restricted to a muscovite–plagioclase-rich layer, present as grains up to 0.3 mm in size that are intergrown with plagioclase and muscovite (Fig. 2); however, K-feldspar is described as a matrix mineral by Goscombe et al. (2015). Similarly, rare magnetite was described by Goscombe et al. (2015), but no Fe–Ti oxides are present in the thin section used for this study (Fig. 2).

Figure 1. **Hand specimen image of sample 198671: garnet-bearing cordierite pelitic gneiss, Mount Narryer**

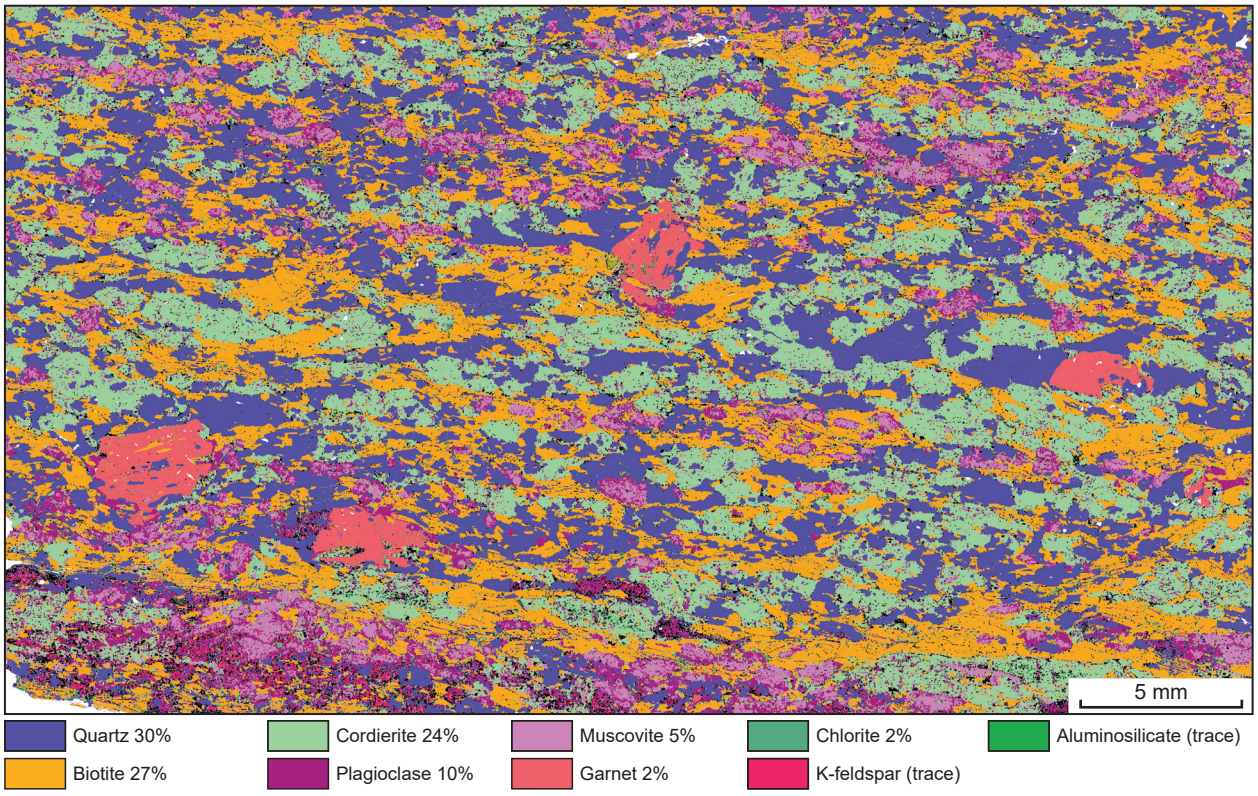

Figure 2. **TESCAN Integrated Mineral Analyser (TIMA) image of an entire thin section from sample 198671: garnet-bearing cordierite pelitic gneiss, Mount Narryer. Volume percent proportions of major rock-forming minerals are calculated by the TIMA software**

Table 1. Mineral modes for sample 198671: garnet-bearing cordierite pelitic gneiss, Mount Narryer

Mineral modes	Grt	Crd	Bt	Sil	Kfs	Ms	Chl	Mag	Ilm	Pl	Qz	Liq
Observed (vol%)	2	24	27	trace	trace	5	2	–	–	10	30	–
Predicted (mol%)												
@ 6 kbar, 830 °C	18.1	13.8	13.2	6.9	15.5			0.9	0.9	6.9	19.1	4.9
@ 5 kbar, 815 °C	10.8	31.8	10.5	–	18.9	–	–	1.7	0.7	8.1	16.6	1.0
@ 5 kbar, 845 °C	19.0	28.7	1.9	–	19.2	–	–	1.1	1.4	5.7	10.7	12.4
@ 4 kbar, 825 °C	9.4	32.5	10.8	–	17.4	–	–	2.1	0.4	8.1	15.6	3.5
@ 6 kbar, 825 °C	17.9	29.2	4.0	–	21.0	–	–	0.7	1.6	6.3	13.4	5.8
@ 5 kbar, 800 °C	10.0	32.0	11.5	–	18.6	–	–	1.7	0.7	8.4	17.1	–
@ 3.4 kbar, 725 °C	5.0	33.9	15.8	–	15.5	–	–	2.2	0.2	9.5	18.0	–

NOTES: – not present

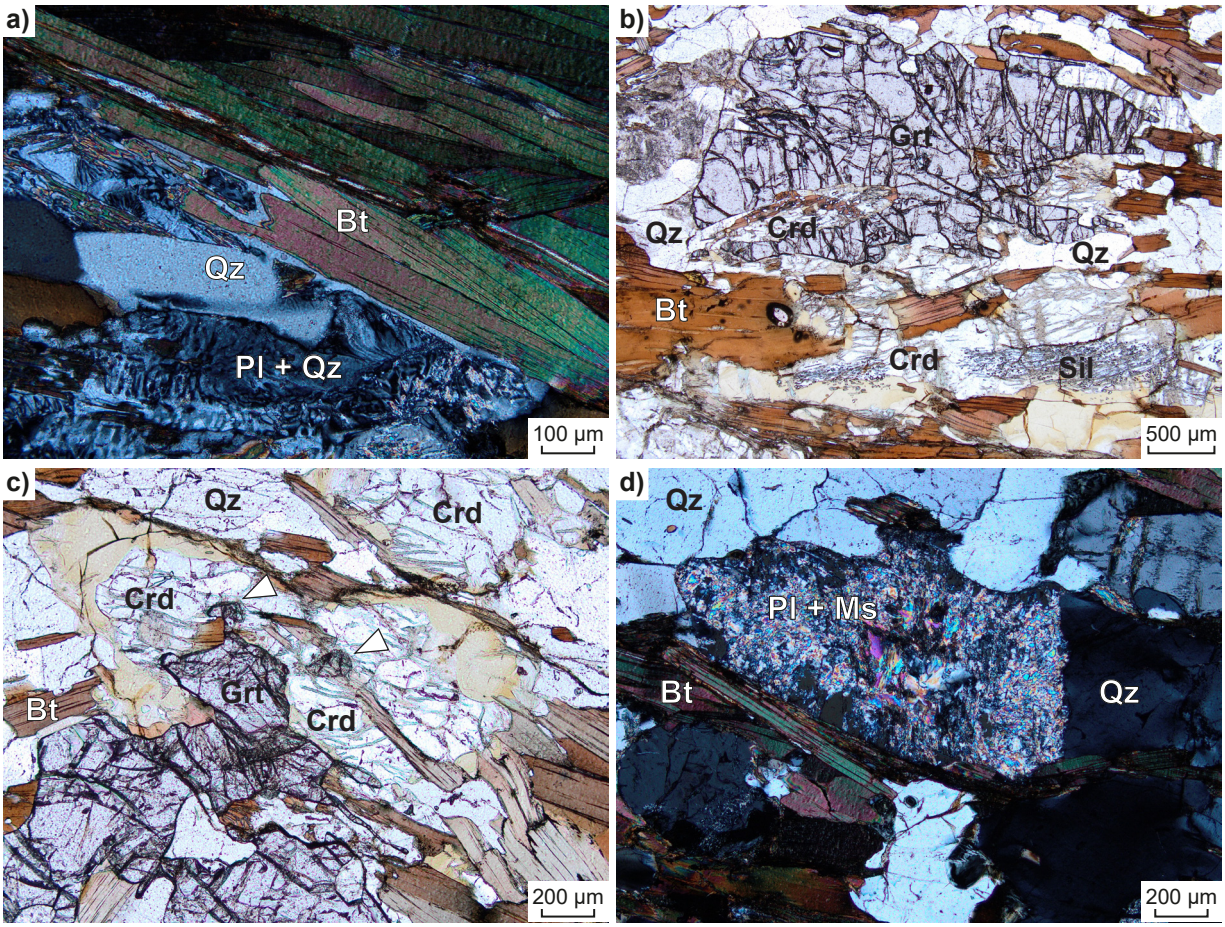

Figure 3. **Photomicrographs, in cross-polarized (a, d) and plain-polarized light (b, c), of sample 198671: garnet-bearing cordierite pelitic gneiss, Mount Narryer. White arrows in (c) point to garnet relics in cordierite. Abbreviations: Bt, biotite; Crd, cordierite; Grt, garnet; Ms, Muscovite; Pl, plagioclase; Qz, quartz; Sil, sillimanite**

Analytical details

The metamorphic evolution of this sample was investigated using phase equilibria, based on the bulk-rock composition (Table 2). The bulk-rock composition was determined by X-ray fluorescence spectroscopy, together with loss on ignition (LOI). The modelled O content (for Fe^{3+}) was assumed to equal 20% of FeO, which stabilized magnetite in exploratory calculations. The H_2O content was reduced from the measured amount of LOI, as higher H_2O contents produce much higher melt volumes than indicated in the sample, and the widespread stability of sillimanite in pseudosections, which is only observed in trace amounts as inclusions in porphyroblasts. The bulk composition was corrected for the presence of apatite by applying a correction to calcium (Table 2). Thermodynamic calculations were performed in the MnNCKFMASHTO (MnO–Na_2O–CaO–K_2O–FeO–MgO–Al_2O_3–SiO_2–H_2O–TiO_2–O) system using THERMOCALC version tc340 (updated October 2013; Powell and Holland, 1988) and the internally consistent thermodynamic dataset of Holland and Powell (2011; dataset tc-ds62, created in February 2012). The activity–composition relations used in the modelling are detailed in White et al. (2014a,b). Additional information on the workflow with relevant background and methodology are provided in Korhonen et al. (2020). Compositional and mode isopleths for all phases were calculated using the software TCInvestigator (Pearce et al., 2015). Additional information on the workflow with relevant background and methodology are provided in Korhonen et al. (2020).

Table 2. Measured whole-rock and modelled compositions for sample 198671: garnet-bearing cordierite pelitic gneiss, Mount Narryer

XRF whole-rock composition (wt%)[a]

SiO_2	TiO_2	Al_2O_3	Fe_2O_3[b]	FeO[b]	MnO	MgO	CaO	Na_2O	K_2O	P_2O_5	LOI	Total
54.00	0.77	20.1	–	10.08	0.21	4.90	1.55	0.44	3.93	0.05	2.45	98.48

Normalized composition used for phase equilibria modelling (mol%)

SiO_2	TiO_2	Al_2O_3	O[c]	FeO^T[d]	MnO	MgO	CaO[e]	Na_2O	K_2O	–	H_2O[f]	Total
59.66	0.64	13.09	0.93	9.31	0.20	8.07	1.76	0.47	2.77		3.10	100

NOTES: (a) Data and analytical details are available from Goscombe et al. (2019)
(b) FeO content is total Fe
(c) O content (for Fe_2O_3) set to be 20% of measured FeO[b]
(d) FeO^T = moles FeO + 2 * moles O
(e) CaO modified to remove apatite: CaO(Mod) = CaO(Total) - (moles CaO(in Ap) = 3.33 * moles P_2O_5)
(f) H_2O reduced from measured LOI; see text

Results

Metamorphic *P–T* estimates have been derived based on detailed examination of the thin section and the bulk-rock composition (Table 2), although there is limited information on the sample volume selected for whole-rock chemistry. The *P–T* pseudosection for this sample was calculated over a *P–T* range of 2–8 kbar and 650–900 °C (Fig. 4). The solidus is located between 790 and 820 °C across the range of modelled pressures. K-feldspar is stable across the entire modelled *P–T* range, and garnet is stable across most of the diagram except at low pressure–high temperature. Sillimanite has a minimum stability of 3.2 kbar at 650 °C, and increases with increasing temperature. Cordierite is stable below 4.1 kbar and 650 °C, with a maximum stability of 7.2 kbar at 875 °C. Orthopyroxene-bearing assemblages are predicted at low pressure–high temperature. Biotite has a maximum stability of 875 °C at 7.2 kbar. Magnetite is not stable at high pressure–high temperature, and ilmenite-absent assemblages are predicted in two wedge-shaped regions, one from 4.1 – 6.2 kbar at 650 °C that decreases in size up to 830 °C, and another between 700 and 795 °C below 3.3 kbar.

Mineral compositions are provided in Table 3. Garnet porphyroblasts are almandine-rich with very slight compositional zoning. Cores have a proportion of almandine [= $Fe^{2+}/(Fe^{2+} + Mg + Ca + Mn)$] = 0.72, pyrope [= $Mg/(Fe^{2+} + Mg + Ca + Mn)$] = 0.13, spessartine [= $Mn/(Fe^{2+} + Mg + Ca + Mn)$] = 0.07, and XFe [= $Fe^{2+}/(Fe^{2+} + Mg)$] = 0.81. Rims have a proportion of almandine = 0.74, pyrope = 0.10, spessartine = 0.08, and XFe = 0.85. Garnet is unzoned in grossular [= $Ca/(Fe^{2+} + Mg + Ca + Mn)$] with contents of 0.05. Plagioclase compositions have Ca(Pl) [= Ca/(Ca + Na + K)] values of 0.77 – 0.78. Biotite compositions have XFe contents of 0.52 – 0.54 and Ti contents of 0.10 – 0.13 per formula unit (pfu). Muscovite is moderately Fe-rich, with XFe = 0.76.

Table 3. Mineral compositions for sample 198671: garnet-bearing cordierite pelitic gneiss, Mount Narryer

Mineral[a]	Crd	Crd	Pl	Pl	Bt	Bt	Bt	Grt	Grt	Grt	Grt	Ms
Setting[b]	Core	Rim	Core	Rim	Core	Rim	Rim	Core	Mantle	Rim	OR	Core
wt%												
SiO_2	48.57	48.55	48.69	48.44	34.94	35.05	33.26	37.22	37.54	37.23	37.20	47.27
TiO_2	0.02	0.00	0.00	0.01	2.31	2.36	1.70	0.00	0.00	0.04	0.01	0.01
Al_2O_3	32.85	33.11	33.32	33.07	19.69	19.74	18.61	21.48	21.35	21.45	21.21	36.62
Cr_2O_3	0.00	0.01	0.00	0.08	0.41	0.32	0.31	0.06	0.12	0.08	0.08	0.03
FeO	8.90	8.55	0.08	0.06	19.58	19.94	21.79	33.06	33.21	33.34	33.96	1.07
MnO	0.26	0.28	0.04	0.00	0.07	0.08	0.18	3.10	3.02	3.35	3.39	0.00
MgO	7.96	8.34	0.00	0.00	9.48	9.05	10.11	4.16	4.09	3.71	3.27	0.19
ZnO	0.04	0.03	0.01	0.00	0.01	0.04	0.00	0.00	0.00	0.00	0.00	0.04
CaO	0.00	0.02	16.25	16.11	0.00	0.00	0.13	1.65	1.70	1.70	1.67	0.07
Na_2O	0.19	0.18	2.71	2.42	0.14	0.19	0.12	0.00	0.00	0.00	0.02	0.07
K_2O	0.02	0.02	0.05	0.07	9.04	9.38	6.82	0.01	0.02	0.03	0.00	10.49
Total[c]	98.82	99.11	101.15	100.25	95.66	96.16	93.02	100.74	101.05	100.93	100.80	95.87
Oxygen	18	18	8	8	11	11	11	12	12	12	12	11
Si	4.98	4.95	2.20	2.21	2.64	2.65	2.59	2.95	2.97	2.96	2.97	3.14
Ti	0.00	0.00	0.00	0.00	0.13	0.13	0.10	0.00	0.00	0.00	0.00	0.00
Al	3.97	3.98	1.77	1.78	1.75	1.76	1.71	2.01	1.99	2.01	2.00	2.87
Cr	0.00	0.00	0.00	0.00	0.02	0.02	0.02	0.00	0.01	0.01	0.01	0.00
Fe^{3+}[d]	0.10	0.15	0.00	0.00	0.06	0.06	0.14	0.08	0.06	0.07	0.06	0.00
Fe^{2+}	0.66	0.58	0.00	0.00	1.18	1.20	1.28	2.11	2.14	2.14	2.20	0.06
Mn^{2+}	0.02	0.02	0.00	0.00	0.00	0.00	0.01	0.21	0.20	0.23	0.23	0.00
Mg	1.22	1.27	0.00	0.00	1.07	1.02	1.17	0.49	0.48	0.44	0.39	0.02
Zn	0.00	0.00	0.00	0.00	0.00	0.00	0.00	0.00	0.00	0.00	0.00	0.00
Ca	0.00	0.00	0.79	0.79	0.00	0.00	0.01	0.14	0.14	0.14	0.14	0.01
Na	0.04	0.04	0.24	0.21	0.02	0.03	0.02	0.00	0.00	0.00	0.00	0.01
K	0.00	0.00	0.00	0.00	0.87	0.90	0.68	0.00	0.00	0.00	0.00	0.89
Total	11.00	11.00	5.00	5.00	7.75	7.77	7.72	8.00	8.00	8.00	8.00	7.00
Compositional variables[e]												
Ca(Pl)	–	–	0.77	0.78	–	–	–	–	–	–	–	–
p(Alm)	–	–	–	–	–	–	–	0.72	0.72	0.73	0.74	–
p(Prp)	–	–	–	–	–	–	–	0.13	0.13	0.11	0.10	–
p(Grs)	–	–	–	–	–	–	–	0.05	0.05	0.05	0.05	–
p(Sps)	–	–	–	–	–	–	–	0.07	0.07	0.08	0.08	–
XFe	0.35	0.31	–	–	0.52	0.54	0.52	0.81	0.82	0.83	0.85	0.76

NOTES: – not applicable
(a) Mineral abbreviations explained in the caption to Figure 4
(b) OR, outer rim
(c) Totals on anhydrous basis
(d) Fe^{3+} contents for biotite assumed to be 10% of Fe total; Fe^{3+} contents for other minerals based on Droop (1987)
(e) Ca(Pl) = Ca/(Ca + Na + K);
proportion of almandine, p(Alm) = $Fe^{2+}/(Fe^{2+} + Mg + Mn + Ca)$;
proportion of pyrope, p(Prp) = $Mg/(Fe^{2+} + Mg + Mn + Ca)$;
proportion of grossular, p(Grs) = $Ca/(Fe^{2+} + Mg + Mn + Ca)$;
proportion of spessartine, p(Sps) = $Mn/(Fe^{2+} + Mg + Mn + Ca)$;
XFe = $Fe^{2+}/(Fe^{2+} + Mg)$

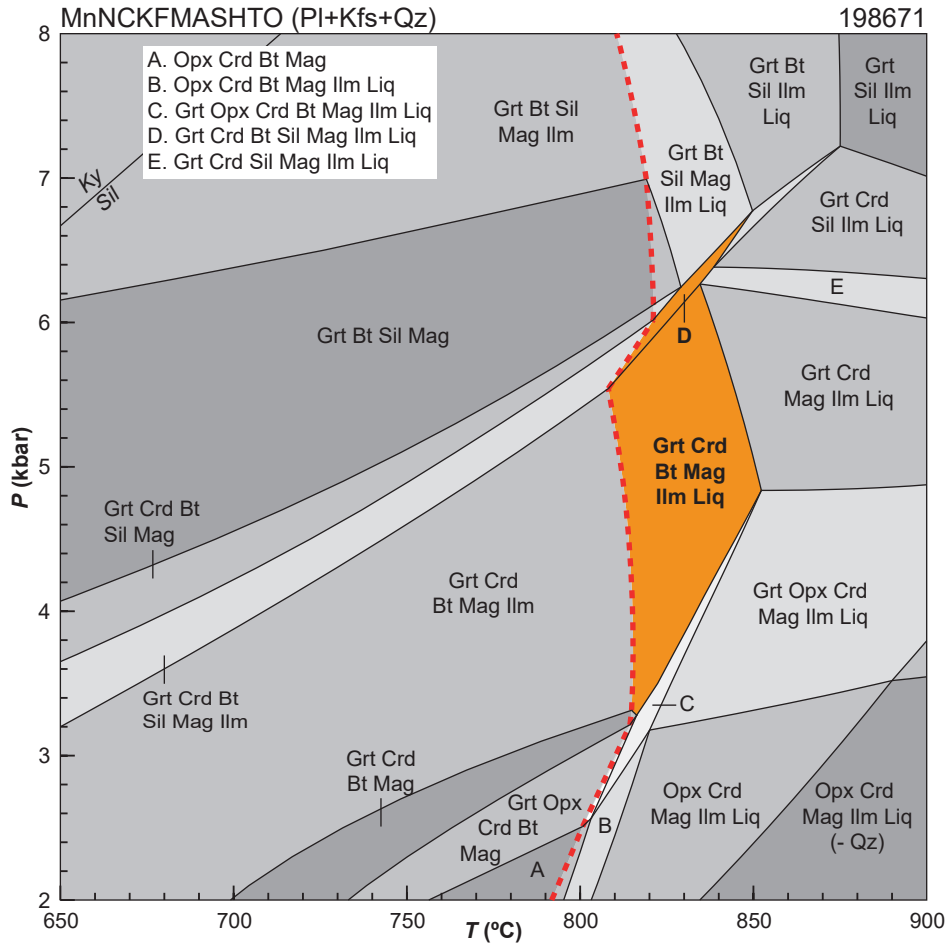

Figure 4. ***P–T*** **pseudosection calculated for sample 198671: garnet-bearing cordierite pelitic gneiss, Mount Narryer. Assemblage field corresponding to peak metamorphic conditions is shown in bold text and orange shading. Red dashed line represents the solidus. Abbreviations: Bt, biotite; Crd, cordierite; Grt, garnet; Ilm, ilmenite; Kfs, K-feldspar; Ky, kyanite; Liq, silicate melt; Mag, magnetite; Opx, orthopyroxene; Pl, plagioclase; Qz, quartz; Sil, sillimanite**

Interpretation

Based on the coarse grain size and mineral associations that support textural equilibrium, the peak granulite-grade metamorphic assemblage is interpreted to contain garnet, cordierite, biotite, quartz and plagioclase. Mineral textures indicate that garnet and cordierite have grown in equilibrium, although the presence of rare garnet relics in cordierite suggests that at least some cordierite growth occurred at the expense of garnet. Sillimanite is only present as inclusions in cordierite and garnet porphyroblasts, so either pre-dates the growth of these porphyroblasts or was in equilibrium with them but was later consumed as garnet and cordierite continued to grow. The hand sample contains only a few mm-scale quartzofeldspathic segregations that may represent leucosome (Fig. 1), represented by the quartz–plagioclase–K-feldspar layer observed in thin section (Fig. 2). Thin films of quartz around biotite are also interpreted to be former melt films. On this basis, a small amount of melt is inferred to be part of the peak assemblage. K-feldspar, magnetite and ilmenite are predicted in the peak assemblage field comprising garnet–cordierite–biotite–plagioclase–quartz–melt; K-feldspar and magnetite are described in this sample by Goscombe et al. (2015) and predicted ilmenite contents in the peak field are generally low (<1.6 mol%, approximately equivalent to vol%; Table 1).

The peak assemblage of garnet–cordierite–biotite–magnetite–ilmenite–plagioclase–K-feldspar–quartz–melt is stable between 810 and 850 °C at 3.3 – 6.2 kbar. Sillimanite is stable with this assemblage in a very narrow field at higher pressure from 5.5 to 6.8 kbar and 810–850 °C. The peak fields are delimited by the solidus at lower temperature, the loss of biotite at higher temperature, the stability of orthopyroxene at lower pressure, and the loss of cordierite at higher pressure. The elevated solidus implies that there has been

some melt loss from the rock volume, although there is uncertainty on the H_2O content most appropriate for the modelling, which affects the temperature of the solidus. Higher H_2O contents than used predict significant melt volumes, stabilize sillimanite and lower the temperature of the solidus; lower H_2O contents elevate the solidus to even more extreme temperatures and destabilize biotite. Although predicted garnet modes in the peak field and the melt-absent field at lower temperature are broadly similar to observed modes (Table 1), there are some discrepancies in the other phases. With little information on the sample volume used for whole-rock chemistry, it is difficult to thoroughly evaluate the possible source of these differences.

Although some textural evolution is preserved in the sample, these microstructures provide little insight into the prograde or retrograde segments of the *P–T* path. The growth of cordierite at the expense of garnet occurs with a decrease in pressure and/or temperature (Table 1), which could record cooling with or without a decrease in pressure. Retrograde muscovite (replacing plagioclase) is not predicted for the bulk composition used in the modelling, which implies that the sample was subsequently hydrated following peak metamorphism. Sillimanite preserved as inclusions in cordierite and garnet could have been in equilibrium with these porphyroblasts (field D on Fig. 4), and would be mostly consumed with a decrease in pressure. Alternatively sillimanite could have been a prograde phase, but the residual composition used in the modelling implies some amount of melt was lost from the protolith, so that the *P–T* pseudosection shown in Figure 4 is not appropriate for investigating the prograde evolution.

Peak metamorphic conditions are estimated at 810–850 °C and 3.3 – 6.8 kbar, with an apparent thermal gradient between 125 and 250 °C/kbar. There is little definitive information on the prograde and retrograde segments of the *P–T* path, and therefore the overall shape of the *P–T* path is not well defined.

References

Droop, GTR 1987, A general equation for estimating Fe^{3+} concentrations in ferromagnesian silicates and oxides from microprobe analyses, using stoichiometric criteria: Mineralogical Magazine, v. 51, no. 361, p. 431–435, doi:org/10.1180/minmag.1987.051.361.10.

Goscombe, B, Blewett, R, Groenewald, PB, Foster, D, Wade, B, Wyche, S, Wingate, MTD and Kirkland, CL 2015, Metamorphic Evolution of the Yilgarn Craton: Geological Survey of Western Australia (unpublished), 910p.

Goscombe, B, Foster, DA, Blewett, R, Czarnota, K, Wade, B, Groenewald, B and Gray, D 2019, Neoarchaean metamorphic evolution of the Yilgarn Craton: a record of subduction, accretion, extension and lithospheric delamination: Precambrian Research, article no. 105441, doi:10.1016/j.precamres.2019.105441.

Holland, TJB and Powell, R 2011, An improved and extended internally consistent thermodynamic dataset for phases of petrological interest, involving a new equation of state for solids: Journal of Metamorphic Geology, v. 29, no. 3, p. 333–383.

Kemp, AIS, Wilde, SA and Spaggiari, C 2019, Chapter 18 — The Narryer Terrane, Yilgarn Craton, Western Australia: Review and Recent Developments, *in* Earth's oldest rocks (2nd edition) *edited by* MJ Van Kranendonk, VC Bennett and JE Hoffmann: Elsevier B.V., p. 401–433, doi:10.1016/B978-0-444-63901-1.00018-6.

Kinny, PD, Williams, IS, Froude, DO, Ireland, TR and Compston, W 1988, Early Archaean zircon ages from orthogneisses and anorthosites at Mount Narryer, Western Australia: Precambrian Research, v. 38, p. 325–341.

Korhonen, FJ, Kelsey, DE, Fielding IOH and Romano, SS 2020, The utility of the metamorphic rock record: constraining the pressure–temperature–time conditions of metamorphism: Geological Survey of Western Australia, Record 2020/14, 24p.

Lu, Y, Wingate, MTD, Kirkland, CL, Goscombe, B and Wyche, S 2015a, 198669: pelitic gneiss, Mount Narryer; Geochronology Record 1288: Geological Survey of Western Australia, 6p.

Lu, Y, Wingate, MTD, Kirkland, CL, Goscombe, B and Wyche, S 2015b, 198654: quartzite, Mount Narryer; Geochronology Record 1287: Geological Survey of Western Australia, 6p.

Myers, JS 1990, Narryer Geniss Complex: Part 1: Summary of the Narryer Gneiss Complex, *in* Excursion guidebook: Third International Archaean Symposium, Perth 1990 (17–21 September) *edited by* SE Ho, JE Glover, JS Myers and JR Muhling: The University of Western Australia, Geology Department and University Extension, Publication 21, p. 62–71.

Myers, J and Williams, IR 1985, Early Precambrian crustal evolution at Mount Narryer, Western Australia: Precambrian Research, v. 27, p. 153–163.

Powell, R and Holland, TJB 1988, An internally consistent dataset with uncertainties and correlations: 3. Applications to geobarometry, worked examples and a computer program: Journal of Metamorphic Geology, v. 6, no. 2, p. 173–204.

White, RW, Powell, R, Holland, TJB, Johnson, TE and Green, ECR 2014a, New mineral activity-composition relations for thermodynamic calculations in metapelitic systems: Journal of Metamorphic Geology, v. 32, no. 3, p. 261–286.

White, RW, Powell, R and Johnson, TE 2014b, The effect of Mn on mineral stability in metapelites revisited: New a–x relations for manganese-bearing minerals: Journal of Metamorphic Geology, v. 32, no. 8, p. 809–828.

Wilde, SA and Spaggiari, CV 2007, Chapter 3.6 The Narryer Terrane, Western Australia: A Review, *in* Earth's Oldest Rocks *edited by* MJ Van Kranendonk, RH Smithies, and VC Bennett, Developments in Precambrian Geology, v. 15, p. 275–304.

Links

Record 2020/14 The utility of the metamorphic rock record: constraining the pressure–temperature–time conditions of metamorphism

Recommended reference for this publication

Korhonen, FJ, Fielding, IOH and Kelsey, DE 2022, 198671: garnet-bearing cordierite pelitic gneiss, Mount Narryer; Metamorphic History Record 25: Geological Survey of Western Australia, 8p.

Data obtained: 28 August 2019

Date released: 7 October 2022

This Metamorphic History Record was last modified on 5 October 2022

Grid references in this publication refer to the Geocentric Datum of Australia 1994 (GDA94). All locations are quoted to at least the nearest 100 m.

WAROX is GSWA's field observation and sample database. WAROX site IDs have the format 'ABCXXXnnnnnnSS', where ABC = geologist username, XXX = project or map code, nnnnnn = 6 digit site number, and SS = optional alphabetic suffix (maximum 2 characters).

Isotope and element analyses are routinely conducted using the GeoHistory laser ablation ICP-MS and Sensitive High-Resolution Ion Microprobe (SHRIMP) ion microprobe facilities at the John de Laeter Centre (JdLC), Curtin University, with the financial support of the Australian Research Council and AuScope National Collaborative Research Infrastructure Strategy (NCRIS). The TESCAN Integrated Mineral Analyser (TIMA) instrument was funded by a grant from the Australian Research Council (LE140100150) and is operated by the JdLC with the support of the Geological Survey of Western Australia, The University of Western Australia (UWA) and Murdoch University. Mineral analyses are routinely obtained using the electron probe microanalyser (EPMA) facilities at the Centre for Microscopy, Characterisation and Analysis, UWA, at Adelaide Microscopy, University of Adelaide, and at the Electron Microscopy and X-ray Microanalysis Facility, University of Tasmania.

Digital data related to WA Geology Online, including geochronology and digital geology, are available online at the Department's Data and Software Centre and may be viewed in map context at GeoVIEW.WA.

Further details of geoscience products are available from:
Information Centre
Department of Mines, Industry Regulation and Safety
100 Plain Street
EAST PERTH WA 6004
Telephone: +61 8 9222 3459 | Email: publications@dmirs.wa.gov.au
www.dmirs.wa.gov.au/GSWApublications